Using a Cylindrical Tactile Sensor for Determining Curvature

Ronald S. Fearing, *Member, IEEE,* and T. O. Binford

Abstract—**This paper shows how contact curvature can be determined from a single contact with a cylindrical tactile sensor. When the tactile finger touches an unknown smooth convex surface, contact location, principal curvatures, and normal force are determined from a 4×4 window of strain measurements. In principle, contact properties can be determined by a linear inverse-filter process, but this approach is inherently doomed by low sampling density and sensor noise. We use a nonlinear model-based inversion from strain measurements back to contact type. Sensor strains are predicted by convolving the spatial impulse response of the rubber skin with the assumed surface pressure distribution derived from a Hertz contact model. Gradient search finds the parameters of the convex second-order shape and the force that best fit the sensor data. Experiments under laboratory conditions show radius estimation within 10%, orientation within 3°, and subtactel (tactile element) localization to 3% of the element spacing. Using a linearized model, we predict error bounds due to sensor noise on the inversion process.**

I. Introduction

Local contact information is important for dextrous manipulation with multifingered hands. Local shape can be defined by second-order surface patches, which are characterized in differential geometry by position, tangent plane, and principal curvatures and their directions. Surface features useful for grasping, such as edges and corners, can be identified by their high curvatures. Knowledge of local curvature is important for finger contact stability [1], [9]. Curvature also provides useful information for object identification and shape description, for example, in vision [24].

There has been little work in determining curvature using tactile sensors. There have been some recent studies in attempting to recover surface pressure profiles with tactile sensors that are relevant to this work. The basic problem with determining surface force distributions is that subsurface strain sensor measurements are a low-passed version of the surface pressure. The elastic impulse-response function of the skin extremely attenuates high spatial frequencies. Speeter [29] simulates determining the radius of a sphere using second differences of the strain profile. Cameron *et al.* [7] propose an inverse filter approach and suggest that the spatial derivatives used in the high-pass filter operation could be obtained by motion of the sensor. Pati *et al.* [23] and Yang [33] examine inverse filtering and regularization approaches to recovering surface stress, using simulated data, and very high density (81 tactile samples) for the two-dimensional problem.

The work mentioned above is useful for recovering an unknown surface stress. However, as we shall see, there is a complicated relationship between surface stress and indentation shape. In many cases it is surface geometry we are interested in as well as the net force on the contact. This paper assumes that the contact stress corresponds to the Hertz contact stress distribution (surface stress is an ellipsoid), and we exploit this constraint with a model-based inverse filter.

Other tactile perception work has not used surface stress determination. Montana [21] suggests finding surface curvature by rolling a sensor without slipping about a contact. (One cannot always afford to roll a finger; the grasp may be disturbed by this motion.) Driels [11] and Shekhar *et al.* [26] found line orientation on a flat array. Brock and Chiu [6] found surface patch orientation using repeated location measurements with a force sensor. Allen and Bajcsy [2] built up a Coons' patch using multiple measurements. The only tactile array curvature experiment found in the literature is Garfinkel *et al.* [20] who used a 3×3 tactile sensor to find curvature using second differences of deflection.

Preliminary work with a cylindrical tactile sensor [14] showed the difficulty of determining the orientation of a rod directly using strain measurements. While a relatively thick skin reduces aliasing and improves localization, information such as contact orientation is distorted.

There are two basic types of tactile sensors: those that measure surface deflection and those that measure subsurface strain. One theoretical advantage of subsurface strain measurement is that deformations can be small; hence, in the valid range for linear elasticity analysis. Practical benefits are that the layer of skin above the sensors reduces aliasing and protects the sensors. With either type of sensor, the local shape measurement is distorted by the compliant skin and non-normal contact forces. The analysis and experiments reported here use a subsurface strain-type sensor.

The obvious approach to surface pressure and deflection recovery is a linear filter. (Curvature is available from surface deflection by fitting a second-order surface.) As we show in the appendix, this method is limited by the low-pass nature of the elastic medium, as we can explain based on simple noise and frequency-response models, and demonstrate with a simple experiment.

Manuscript received February 17, 1989; revised April 15, 1991. This work was supported by DARPA under Contract MDA903-86-K-0002. Portions of this paper were presented at the IEEE International Conference on Robotics and Automation, Philadelphia, PA, 1988.

R. S. Fearing is with the Department of Electrical Engineering and Computer Science, University of California, Berkeley, CA 94720.

T. O. Binford is with the Department of Computer Science, Stanford University, Stanford, CA 94305.

IEEE Log Number 9101932.

To overcome the disadvantages of the linear-filter approach, a contact-model-based method is developed. By using an *a priori* constraint on the contact type, which is assumed to be locally convex and elliptical, umbilical, cylindrical, or planar, the problems of the linear filtering approach can be avoided. This model-based approach uses a nonlinear inversion of sensed strain to obtain surface shape. We assume frictionless indentation and then, using the Hertz contact assumption, the measured strain can be predicted for a given contact type. We show that this relationship is numerically stable and thus invertible. The inversion is done by numerical search and has been tested experimentally for various sizes of cylinders and spheres, including point and line contacts.

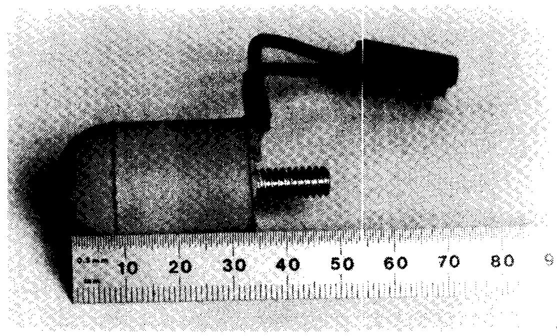

Fig. 1. Tactile sensing finger for the Stanford/JPL hand.

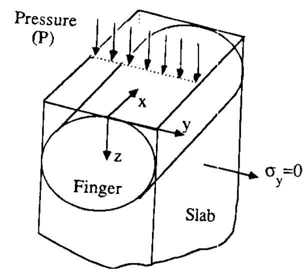

Fig. 2. Geometrical approximation for plane-stress model.

II. Sensor Implementation

The tactile sensor array is packaged in a molded rubber finger tip (Fig. 1). The finger is a 25.4-mm-diameter cylinder approximately 25 mm long with a hemisphere on the tip. The finger tip sensor uses an array of capacitors formed at junctions of perpendicular copper strips, spaced at 3.3 mm along the length and 18° around the circumference of the cylindrical portion, of which an 8×8 subset is used. Rubber 3.8 mm thick covers the core and is essential to increase contact areas and reduce aliasing [12]. The rubber dielectric layer is a molded hollow structure (the inverse of [27]). Details of finger construction are in [13] and [16]. Other cylindrical fingers are described in [2], [4], and [10].

After calibration, the sensor output is normalized to determine equivalent strain at each tactel (tactile element). The mean sensitivity of the tactels is 4 mN with a 3-mm-diameter probe, and they are very linear up to 0.5-N load. (The sensor is linear to within 4 mN in the 0–0.5 N range, but only within 30 mN in the 0–1 N range.)

III. Impulse Response Model

For an ideal linear tactile sensor, the strain beneath the surface of the skin is determined by the convolution of the surface pressure with the elastic material's spatial impulse response. To determine contact pressure from these strain measurements requires some form of deconvolution operation. The spatial impulse response is difficult to analyze for complicated geometries, such as this finger; thus, we use an empirical rather than analytic impulse-response model. To get an initial model estimate, we make some gross approximations and consider a simplified planar elasticity problem. An elastic strip model [18] could be used for the sensor capacitor above the hard finger core, but the shape of the impulses are approximately the same.

Consider a slice of elastic material in the x–z plane with the applied force per unit length constant in the y direction and stresses on the face $\sigma_y = 0$. This "plane-stress" approximation is shown in Fig. 2. For a normal line load on a linear isotropic medium, the z component of strain (ϵ_z) is [32]:

$$\epsilon_z(x, z = d) = \frac{-2Pd}{E\pi r^4}\left[d^2 - \nu x^2\right] \qquad (1)$$

where P is the force per unit thickness of the slab in Nm^{-1} s, E (Nm^{-2}) is the elastic modulus (stress per unit strain), ν is Poisson's ratio, d is the sensor depth, and $r^2 = d^2 + x^2$. Equation (1) is the one-dimensional impulse response. By convolving the impulse response with a surface force distribution $p(x)$, the z component of strain can be determined.

To experimentally determine the one-dimensional impulse response, an approximate line load of 0.5 N was applied normally at 0.64-mm steps along x while recording one tactel (dots in Fig. 3). Depth and Poisson's ratio parameters in (1) were adjusted to best fit the normalized samples in the least squares sense, obtaining $d = 3.8$ mm and $\nu = 0.4$. The solid curve in Fig. 3 is the plane-stress model with these parameters, not an arbitrary best fitting curve. The root-mean-squrae (rms) fitting error is 1.3% of full scale. For a central region of 4×8 tactels, away from the tip, the rms error is between 1.27% and 2.4% with mean rms fitting error of 1.9%. The sensor agrees closely to the model, in spite of violating the small deflection assumption of linear elasticity (peak strain with this load is on the order of 10%).

When the contact pressure is not constant along the width of the contact, a two-dimensional impulse response $h(x, y)$ can be convolved with surface pressure $p(x, y)$ to obtain the subsurface strain $\epsilon_z(x, y, d)$. To model the two-dimensional impulse response, the cylinder is approximated by the tangent plane at the contact point (Fig. 4). The equivalent sensor spacing in the y direction is $r_f \sin \Delta\theta = 3.9$ mm, for angular spacing ($\Delta\theta$) of 18°, where $r_f = 12.7$ mm is the finger radius. By applying a small hemispherical probe at 0.635 mm $\times$ 0.635 mm spacing along the x and y axes, 12×11 measurements were obtained. The measured impulse response is not circularly symmetric with respect to its peak. We do not have a theoretical model for the strain in the

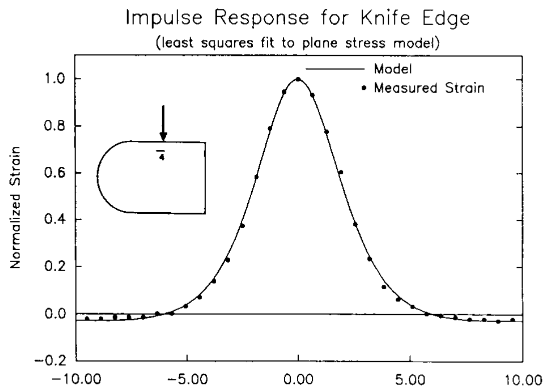

Fig. 3. Plane stress model and experimental data.

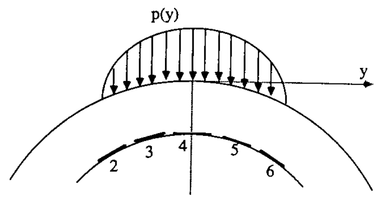

Fig. 4. Sensor geometry around finger circumference.

cylinder, but an empirical separable impulse response

$$h(x, y) = h_x(x) h_y(y) \tag{2}$$

worked well. For this model, we assume a response of the form of the plane-stress equation in the x and y directions

$$h_x(x) = \frac{d_x^2(d_x^2 - \nu_x x^2)}{(x^2 + d_x^2)^2} \tag{3}$$

$$h_y(y) = \frac{d_y^2(d_y^2 + \nu_y y^2)}{(y^2 + d_y^2)^2} \tag{4}$$

where d_x, d_y and ν_x, ν_y are equivalent depth and Poisson's ratio parameters, respectively, along the cylinder axis and around the circumference. Depth and Poisson's ratio parameters were adjusted to minimize mean square error between (2) and the normalized samples, obtained $d_x = 4.3$ mm, $\nu_x = 0.5$, $d_y = 6.0$ mm, and $\nu_y = 0.7$. Because we are using a spherical load instead of a line load, the strain response will no longer have the symmetry required for the plane-stress assumption to hold. Values of Poisson's ratio in this model > 0.5 are not physically significant. However, it is interesting to note that a simple substitution $\nu^* = \nu/(1 + \nu)$ [18] can be used to convert the plane elasticity expression from plane stress to plane strain. Thus, $\nu_y = 0.7$ with plane stress corresponds to $\nu_y^* = 0.4$ with plane strain. Fig. 5 shows deflection contours over the centralized 8×8 samples comparing normalized model and experimental data. The rms error of the sample fit was 2.0% of full scale. Note that any other *ad hoc* model for the impulse response could have been used instead; however, our choice was made to maintain

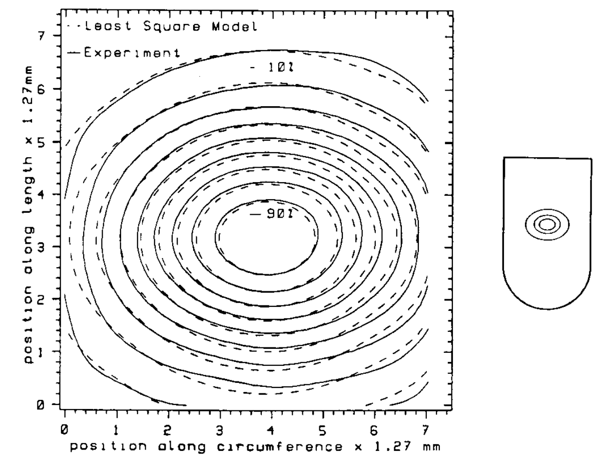

Fig. 5. 2D model and experimental impulse response.

some connection with the physics of the sensor. The Boussinesq function, which is the strain response for a half space with point load [17], [18] is circularly symmetric, and thus is not a good choice for the impulse response model.

IV. Determining Contact Shape

We want to determine curvature of a C^2 rigid indentor pressing into a compliant finger. We need to know the contact pressure distribution, and in this section the shape of the contact region is determined for this restricted class of indentor. If we wish to determine the contact pressure or shape more accurately than possible with a linear inverse filter, we need to use a constraint on the form of contact.

We use the classical Hertz contact approximations [32]. The bodies are locally smooth and large with respect to indentation depth and contact size. Contacts are small compared to the finger radius. The indentation is frictionless. Local yielding is ignored; we assume that contact occurs only on the surface of the finger.

The finger cylinder is approximated locally by a parabola:

$$z_f \approx C_f y^2 \tag{5}$$

where $C_f = -1/2R_f$, with R_f the finger radius (12.7 mm). (The finger axes are shown in Fig. 2). The body indenting the finger is represented by

$$z_B = A_B \tilde{x}^2 + C_B \tilde{y}^2 + \delta \tag{6}$$

where $\tilde{x}$, $\tilde{y}$ are principal curvature plane axes, δ is the indentation depth, $A_B = 1/2R_B$, and $C_B = 1/2R'_B$, with R_B and R'_B principal radii of curvature of the indenting body.

Rotating by the angle ψ from indentor to finger coordinates in (6), where ψ is defined in Fig. 6, and setting $z_f = z_B$ (the two surfaces are intersecting), we obtain

$$x^2[A_B c^2\psi + C_B s^2\psi] + 2xyc\psi s\psi[A_B - C_B] + y^2[C_B c^2\psi + A_B s^2\psi - C_f] = \delta \tag{7}$$

where $c\Psi = \cos\psi$, and $s\psi = \sin\psi$. Substituting $A =$

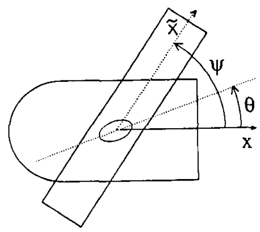

Fig. 6. Cylinder contact on finger (top view).

$A_B c^2\psi + C_B s^2\psi$, $B = 2(A_B - C_B)c\psi s\psi$, and $C = C_B c^2\psi + A_B s^2\psi - C_f$, we see that (7) is an ellipse:

$$Ax^2 + Bxy + Cy^2 = D. \tag{8}$$

This contact ellipse has its major axis at the angle given by θ [31] (Fig. 6) where

$$\tan(2\theta) = \frac{B}{A - C} = \frac{(A_B - C_B)\sin 2\psi}{(A_B - C_B)\cos 2\psi + C_f}. \tag{9}$$

For a cylindrical indentor, $A_B = 0$.

Equation (8) is rotated by θ to obtain the major and minor axes of the contact ellipse:

$$z_f = A' x'^2 + C' y'^2 \tag{10}$$

with

$$A' = Ac^2\theta + Bs\theta c\theta + Cs^2\theta$$
$$C' = As^2\theta - Bs\theta c\theta + Cc^2\theta.$$

If the radius of a cylindrical indentor (R'_B) is large with respect to the radius of the finger (R_f), the orientation of the contact ellipse (see (9)) no longer corresponds to the orientation of the contacting cylinder. Thus, the contact ellipse orientation cannot be used directly to determine an indenting cylinder's orientation.

V. Contact Pressure

The pressure distribution corresponding to a frictionless contact between two paraboloids is an ellipsoid [18]:

$$p(x', y') = \frac{3F}{2\pi ab}\sqrt{1 - \frac{x'^2}{a^2} - \frac{y'^2}{b^2}} \tag{11}$$

where a and b are the major and minor axis of the ellipsoid at $z = 0$, F is total force, and $p(x', y') = 0$ outside the contact area. (Fig. 4 shows the ellipsoidal pressure distribution in cross section.) The length of the major axis of the contact ellipse [32] is

$$a = m(A', C')\left(\frac{3F(1 - \nu^2)}{(A' + C')E_f}\right)^{1/3} \tag{12}$$

where E_f is the elastic modulus of the finger, and it is assumed that we have a rigid body and a soft finger. The factor $m(A', C')$ is determined from the solution of the elastic deflection equation [18], which gives the contacting ellipse size. The solution uses the complete elliptic integrals of the first and second kind and is tabulated in [8] as a function of eccentricity of the contact ellipse. The minor axis of the ellipse is given by

$$b = a\sqrt{1 - e^2} = \sqrt{1 - \left(\frac{A'}{C'}\right)^2} \tag{13}$$

where e is the eccentricity.

The elliptical contact can now be predicted for a rigid cylinder pressed into the cylindrical finger. (Throughout the paper, we use $E_f \approx 2.5 \times 10^5$ Nm^{-2}, the approximate value of Young's modulus for our sensor.) For example, a 10-mm-radius cylinder with its axis at 45° to the sensor pressed with $F = 1$ N gives a contact ellipse of 11.4 mm × 3.5 mm, oriented at 26° from the x axis. (This ellipse will fit inside a 2 × 2 window of tactels—much smaller than minimum sampling requirements). Contact ellipses are plotted in Fig. 7 at 15° increments in cylinder orientation (along ordinate) and six different radii (along abscissa) for 1 N of force. A line is drawn to show scale.

This ellipse calculation breaks down for parallel axes, and a different formulation is needed; see [18]. Another limitation is that a predicted contact ellipse may be longer than the finger because the analysis assumes infinite-length finger and indentor cylinders. Although our method does not handle this case, when the contact becomes very long compared to the finger length, the surface stress will be approximately constant along any cross section orthogonal to the finger axis, and a two-dimensional plane-strain analysis should be valid. The contact stresses for a cylindrical finger pressing against a plane were discussed in [12].

VI. Curvature from Strain

If one can predict measured strain as a function of the contact condition, in principle the function can be inverted to obtain the contact conditions as a function of the strain. Estimated sensor strain in the model is obtained from convolution of the sensor impulse response of (2) with the ellipsoidal pressure distribution of (11):

$$\hat{\epsilon}_z(x, y) = h(x, y) starp(x, y) \tag{14}$$

where the planar approximation from Section III is used. The equations are outlined as:

$$\begin{pmatrix} R_B, R'_B, \psi, F \\ \text{contact} \\ \text{parameters}\end{pmatrix} \rightarrow \begin{pmatrix} a, b, \theta, P \\ \text{ellipsoid} \\ \text{parameters}\end{pmatrix}$$
$$\rightarrow \begin{pmatrix} h(x, y) \\ \text{impulse} \\ \text{response}\end{pmatrix} \rightarrow \hat{\epsilon}_z(x, y) \tag{15}$$

where $\hat{\epsilon}_z$ is the predicted strain. Using the *a priori* constraint that the contact is a paraboloid, we want to invert (15) to obtain contact parameters from measured strain values.

The tactile sensor discrete samples are represented by an array

$$\epsilon_z[m, n] = \epsilon_z(m\Delta x, n\Delta y) \tag{16}$$

where $\Delta x \approx 3.3$ mm and $\Delta y \approx 3.9$ mm are the sensor

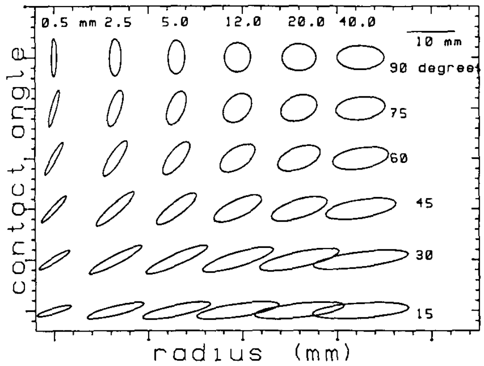

Fig. 7. Contact ellipses for cylindrical indentors (to scale) for 1-N load.

spacing (using the planar sensor approximation). We quantify the quality of fit between model and experiment by a normalized sum of squares. The mean square error (MSE) between model and experimental values is calculated for a 4×4 region of the array that contains the peak strain value:

$$\begin{aligned} \text{MSE} &= \xi^2 \\ &= \frac{1}{4 \times 4} \frac{1}{\max \epsilon_z} \sum_n \sum_m \left(\hat{\epsilon}_z[n, m] - \epsilon_z[n, m] \right)^2. \end{aligned} \tag{17}$$

This expression is normalized by the maximum strain measured on the sensor; thus, ξ corresponds to the rms (error) of the fit of all elements to the model as a percentage of the peak strain.

The modeling error ξ is minimized by a gradient search technique, where the set of parameters for a cylinder is $[R_B, F, \psi, x_o, y_o]^T$, including the center position of the contact x_o, y_o. The search is started from the interpolated center of pressure, which corresponds to the peak strain location [13]. The interpolation error due to aliasing is ± 0.4 mm along x and ± 0.5 mm along y. The gradient adjustment of position for best rms fit eliminates the systematic interpolated position error.

For this initial work, the goal is to recover curvature from the cylindrical tactile sensor—not to extract it in the most computationally efficient manner—so slow convergence of the gradient method is not a major concern. (Typical times were several minutes on a VAX 11/750.) The error surface was examined for several cases and found to be bowl-shaped locally, so techniques such as Newton's Method could give faster convergence. In experiments, the gradient search (with initial parameters far away from the true values) converges to the desired values, albeit slowly in some trials. The search did not get stuck in local minima; however, we have no formal proof of global convergence of the search. The search was concluded when $\Delta\xi / \xi$ was $< 10^{-4}$.

VII. Sensitivity to Error

Good conditioning of the inversion is important for useful results to be obtained. We examine cylinder radius and orientation estimation limits due to sensor noise. Impulse response modeling errors and limitations from the planarity and frictionless indentation assumptions are neglected, but in practice these systematic biases are more significant than the random errors. However, this simplified linear analysis allows us to make an estimate of the inversion process sensitivity to error.

We assume an additive noise model for the measured strain ϵ_z

$$\epsilon_z = \hat{\epsilon}_z + \Delta\epsilon_z + \eta \tag{18}$$

where $\Delta\epsilon_z$ is noise and η is systematic model error. The model error includes geometric effects, possible friction effects, and contact assumptions that are violated. In experiments we found that the dominant sensor noise with no load is due to quantization [15]. The strain signal has quantization steps ($\delta\epsilon_z$) of 0.1% in dimensionless strain units ($\delta\epsilon_z = \pm 0.05\%$), corresponding to 3-mN force sensitivity with a 3-mm-diameter probe. We make the common assumption that quantization errors from analog-to-digital conversion can be modeled as a random process with uniform distribution [22, p. 415]: the samples' amplitudes vary widely over the 4×4 array compared to quantization step size. Probe noise was not spatially independent and appears as an error in applied force, which affects all tactels in a correlated manner. Random friction effects, while harder to quantify, seem to be less significant than quantization.

We define two error vectors: the parameter estimation error

$$\Delta\underline{R} = (\Delta R_B, \Delta\psi, \Delta F)^T \tag{19}$$

and the sensor error

$$\Delta\underline{\epsilon}_z = (\Delta\epsilon_{z11}, \Delta\epsilon_{z22}, \cdots, \Delta\epsilon_{z43}, \Delta\epsilon_{z44})^T. \tag{20}$$

We want to determine max $\Delta\underline{R}$, the maximum expected error in the radius, force, and orientation estimates as a function of max $\Delta\underline{\epsilon}_z$, the worst case strain sensor error. The measured normal strain is represented as a vector function $\underline{f}()$

$$\underline{\epsilon}_{z0} = \underline{f}(R_0, \psi_0, F_0). \tag{21}$$

Since strain is a continuous function of the contact parameters, for small strain errors, $\underline{f}$ can be expanded in a Taylor's series about nominal values:

$$\underline{\epsilon}_z \approx \underline{\epsilon}_{z0} + \Delta\underline{\epsilon}_z = \underline{\epsilon}_{z0} + J\Delta\underline{R} \tag{22}$$

where J is the Jacobian of $\underline{f}()$. For a 4×4 array of sensors, J is a 16×3 matrix. The least squares matrix solution [30] for $\Delta\underline{R}$ is

$$\Delta\underline{R} = (J^TJ)^{-1} J^T \Delta\underline{\epsilon}_z = J^+ \Delta\underline{\epsilon}_z \tag{23}$$

where $J^+ = (J^TJ)^{-1}J^T$ (the pseudoinverse). J^TJ is well conditioned for the measurement range used here. With independent, identically distributed noise, the parameter covariance matrix is

$$\Lambda_R = J^+\sigma_\epsilon^2 I J^{+T} = J^+J^{+T}\sigma_\epsilon^2 = \sigma_\epsilon^2(J^TJ)^{-T} = \sigma_\epsilon^2(J^TJ)^{-1} \tag{24}$$

where σ_ϵ^2 is the individual sensor noise variance. (Note that J^TJ is symmetric.)

Given bounds on expected sensor error ($\Delta \underline{\epsilon}_z$), the worst case expected error for each parameter is found independently. Examining the rows of J^+, the maximum parameter change in each element of $\Delta \underline{R}$ will occur when $\Delta \underline{\epsilon}_z$ is aligned with $\underline{J}_i^+$, the ith row of J^+, that is

$$\max(\Delta R) = \max(\underline{J}_1^{+T} \Delta \underline{\epsilon}_z)$$
$$= \underline{J}_1^{+T}\left(\frac{\underline{J}_1^+}{|\underline{J}_1^+|}|\Delta \underline{\epsilon}_z|\right) = |\underline{J}_1^+||\Delta \underline{\epsilon}_z|. \quad (25)$$

Similarly, $\max \Delta\psi = |\underline{J}_2^+||\Delta \underline{\epsilon}_z|$ and $\max \Delta F = |\underline{J}_3^+||\Delta \underline{\epsilon}_z|$. The length of the sensor error vector is simply

$$|\Delta \underline{\epsilon}_z| = \sqrt{\Delta \underline{\epsilon}_z^T \Delta \underline{\epsilon}_z} \leq \sqrt{N}\,\delta\epsilon_z \quad (26)$$

with N the number of tactels in the window. Thus, $|\Delta \underline{\epsilon}_z| \leq 0.2\%$. Note that error sensitivity may not be uniform. That is, the rows of J^+ could be $\underline{J}_i^{+T} = [0 0 0 \cdots 1 0 0]$, with all parameter sensitivity due to error at a single tactel. However, the rubber skin spreads strain to all sensor sites, and thus in practice error sensitivity is well distributed over the central tactels in the window.

Maximum bounds on each parameter are directly related to the covariance matrix. That is, max $\Delta R, \Delta\psi$, and ΔF are the diagonal elements of JJ^{+T}, the covariance matrix (24). The relation between the error bound and the standard deviation of any estimate is thus just a scale factor (for a uniform distribution):

$$\frac{\Delta R}{\sigma_R} = \frac{\delta\epsilon_z\sqrt{N}}{2\,\delta\epsilon_z/\sqrt{12}} \approx 6.93. \quad (27)$$

Contact parameter-estimation error bounds are also affected by the least squares fit of (17). For example, when the two-dimensional impulse-response model was determined, there was a fitting error of 2% of full-scale rms between the experimental data and the model. The peak strain is about 15% for a 0.5-N load, thus the normalized $|\Delta \underline{\epsilon}_z|$ in terms of full scale was 1.3% (4 $\delta\epsilon_z/15\%$). The expected error due to quantization would be much less than 1.3% of full scale; thus, the impulse model error contains more systematic error than sensor quantization error. This systematic error will not generally lie in the direction of $\underline{J}_i^+$, so it will tend to place an overly high estimate on parameter error if used in (25). It would be more reasonable to assume that the systematic error is uniformly distributed over the tactel window.

A. Error Dependence on Applied Force

Parameter estimation error bounds are evaluated using quantization noise. Predicted errors in radius and orientation estimation are numerically calculated as a function of force for cylinders at 90° to the finger axis, with the contact location half way between tactels (Figs. 8 and 9). Better performance is predicted with increased contact force (improved S/N ratio), and thus greater tactel output and larger contact area. According to Fig. 8, radius estimates would not be usable unless the force is greater than about 0.5 N. Angle error would be reduced with a smaller diameter cylinder, which is expected because the contact ellipse becomes more eccentric, making orientation less ambiguous.

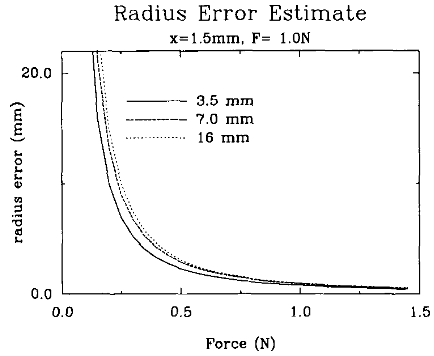

Fig. 8. Force dependence of radius error sensitivity.

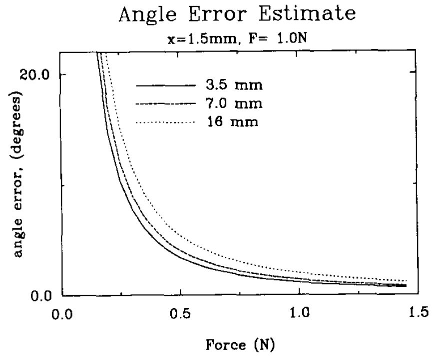

Fig. 9. Force dependence of angle error sensitivity.

The bound on force error ΔF was calculated as a function of applied force and cylinder radii (not shown). Interestingly, the force error is predicted to be relatively independent of force, radius, or angle of the contacting cylinder, and has bound of ± 15 mN.

B. Error Dependence on Cylinder Orientation

Figs. 10 and 11 show the error bounds as a function of the indenting cylinder's orientation in the range from 30° to 150°, for 1-N force. In the central region (axes perpendicular), we expect less than 10% error in radius for the 12.5-mm-radius cylinder. The errors increase as the cylinder and finger axis get closer to alignment because the contact ellipse representation is singular for parallel axes.

An interesting feature is the jagged appearance of the error bounds, which is due to two effects, angle quantization with a rectangular sampling grid [19] and the zeros of the impulse response. As a cylinder rotates on the surface of the finger, the zero crossings of its strain response will be directly above certain tactels; that element can have no effective contribution to the parameter estimation. There is a blip in the orientation estimate for the 12.5-mm-radius cylinder perpendicular to the finger. The contact ellipse becomes close to circular here; a small change in angle distorts the circle more noticeably in this orientation (see Fig. 7).

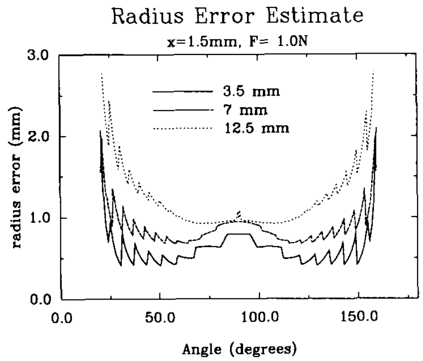

Fig. 10. Angle dependence of radius error sensitivity.

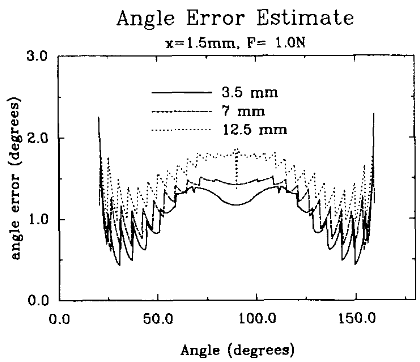

Fig. 11. Angle dependence of angle error sensitivity.

C. Localization Errors

The position sensitivity can also be predicted in the same manner. The worst case predicted error for a 14-mm-diameter cylinder pressed against the finger at 90°, $|\underline{J}_x^{+T}|\,|\Delta\underline{\epsilon}_z|$, was found to be $\Delta x \leq 0.03$ mm. This position error is just 1% of the tactel element spacing along the finger length. Localization of a line contact, using the analytic expressions from the plane stress model for the strain due to a line contact, has localization errors in the range of 1% for 1% sensor error, so this result is not unexpected. (If the contact were known to be a line contact, the outputs of just two sensor elements could be used to determine the line contact location. Here we have more sensor elements to use.)

D. Finger Sensitivity Threshold

This same error analysis provides a tool to quantify the minimum detectable force for a finger touching a flat surface, which will be the most sensitive type of contact. We want to look at the standard deviation of the force estimate σ_F. Note that the contact area increases with increasing force, and the contact will be a line contact at low forces. The standard deviation of the force estimate, from (24), is

$$\sigma_F = \sigma_\epsilon \sqrt{[J^+ J^{+T}]_{33}} \tag{28}$$

where we have selected the diagonal element of Λ_R as the force variance.

The flat contact analysis was approximated by a large-radius cylinder indenting the finger at 90°. A cylinder with 1500-mm radius and 0.05-N force had a predicted contact ellipse length of 10.7 mm and width of just 0.53 mm. A larger radius or contact force would cause the contact ellipse to exceed the finger length, hitting a representational singularity in the analysis. The estimated force was found to have a fairly constant $\sigma_F \approx 1.3$ mN for very small forces and a wide range of cylinder diameters. The standard deviation of the force (σ_F) is about the same as the standard deviation of each tactel; apparently the predicted line contact from the flat contact did not increase the contact area sufficiently to allow averaging of more tactels.

VIII. Experimental Results

A single set of experiments was performed using one calibrated version of the tactile sensor, and the results are reported here. For the same input conditions, the output was consistent. While statistics from multiple experiments under same input conditions have not been performed, estimation errors were near the worst case prediction, implying that unmodeled systematic error was significant.

Curvature estimation was tested by pressing a cylindrical probe normally into the finger sensor and sequentially reading all elements in the 8×8 tactel array in approximately 0.1 s. The strains were linearized by a lookup table. The residual sensor strain (hysteresis) was zeroed before each measurement. A Delrin or aluminum probe was attached to a balance beam, and the applied force was controlled to 5% by the weight on the beam. The finger was mounted on a machinist's table and positioned under the probe. The table was accurate to 25 μm in translation and about 0.1° in rotation.

The low-pass property of the skin complicates extracting angle and radius information from strain. Fig. 12 shows contours of constant strain for a 25-mm-diameter cylinder applied at 70° with 1-N force. The strain contours are a distorted version of the surface pressure and do not appear to directly contain information of the indenting cylinder's diameter and orientation. Thus, it seems that simple heuristic methods for determining curvature, such as calculating moments of strain measurements, are not likely to be very successful. Note that a 4×4 window of strain measurements, as used in our algorithm, covers most of the significant portion of the strain pattern.

The four impulse response parameters (d_x, d_y, ν_x, ν_y), the modulus of elasticity E, and the sensor spacing (determined from design parameters 3.3 mm and 18°) are not adjusted by the gradient search. The model parameters are determined from design values and independent sensor characterization experiments.

A. Cylinder Diameter

For this set of measurements, cylinders were applied orthogonally to the finger above tactel [2 4] to eliminate cell variation effects. Section VIII-C demonstrates that force and radius estimation are position independent. Fig. 13 shows sensed versus actual cylinder diameter (details in Table I). Radius errors are < 1 mm, which agrees with the error bound of Fig. 8, except for the 66-mm-diameter cylinder.

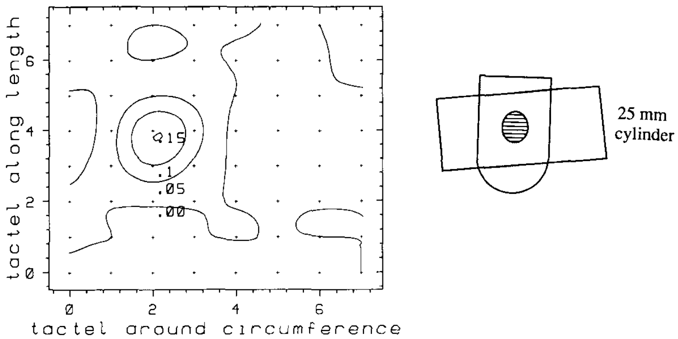

Fig. 12. Strain contours for 25-mm cylinder at 70°.

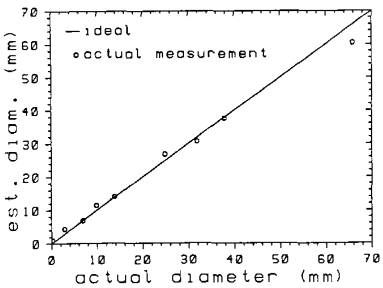

Fig. 13. Estimated cylinder diameter for $\psi = 90°$.

TABLE I
DETERMINING CYLINDER DIAMETER FOR CONTACT AT 90°

Diam. (mm)	Force (N)	Est. Diam.	Est. Force	rms error
0.3	0.5	1.1	0.42	3.09%
3	0.5	4.5	0.49	2.78%
7	1.0	7.0	0.96	2.15%
10	1.0	11.6	1.09	2.95%
14	1.0	14.2	0.91	1.56%
25	1.0	27.0	1.02	1.78%
32	1.0	30.8	1.07	1.69%
38	1.0	37.7	1.19	2.11%
66	1.0	60.6	1.16	2.16%

The 66-mm-cylinder contact ellipse is 9.9×5.5 mm, which may be too wide for the planar finger approximation to be valid. Force is estimated within about 10% except for larger diameters, but the error analysis predicts $\Delta F < 0.015$ N. Gain variations from calibration may cause this error.

If estimates are close to the "maximum" error, then systematic error in the sensor model has more effect than quantization. A refined, higher order model for the sensor would consider the sources of these residual errors. For example, every tactel could have its own individual impulse response model, and a position calibration could be used to locate exactly the placement of all cells. This refined model could then compensate for manufacturing variations.

The rms error (ξ) in Table I suggests how well the gradient search fit a paraboloid indentor (processed through (15)) to the 4×4 set of strain measurements for each contact. An rms error of $< 3\%$ of full scale is good compared to the 2% rms fitting error for the impulse response of Section III, and here there are additional error sources such as cell-to-cell variations. Better fit (lower rms error) seems to be correlated with better radius estimation.

The estimated contact ellipse width $a = 2.25$ mm for the 10-mm-diameter cylinder contact is smaller than the 3.3-mm sensor spacing. This subtactel "resolution" is possible because the surface deflection is a second-order function, and thus the space of possible strain functions is constrained.

B. Cylinder Orientation

Determining the local orientation of objects on a finger is perhaps more useful than radius estimation. (For example, controlling the attitude of a part in a robot hand could use the orientation information.)

Good angle estimation was obtained with a 25-mm-diameter cylinder (Fig. 14). For these experiments the cylinder was applied with 1-N force at a random position, not above element [2 4]. The random position did not reduce accuracy; the angle error $\Delta\psi$ ($\pm 3°$ near 90°) was within the predicted bounds of Fig. 11. Radius estimates were unreliable as the cylinder axis became close to the finger axis. Here the predicted contact ellipse extended beyond the finger cylinder ends, but was still aligned with the tactile samples for best fit. Fig. 15 shows the poor radius estimation obtained when the cylinder orientation was not within about 45° of perpendicular to the cylindrical sensor axis.

C. Position Independence

It is important to characterize the variation in estimation quality with contact position on the sensor. Variation with contact position should identify inhomogeneities in sensor fabrication or calibration.

A 14-mm-diameter cylinder perpendicular to the finger was moved along the finger (x) axis in 0.381-mm steps, and the plot of sensed and ideal location is shown in Fig. 16. Residual errors were $< \pm 0.1$ mm, or just 3% of the tactel spacing. Since the sensor was hand fabricated, the sensor spacing may be 3.2 mm instead of the nominal design value of 3.3 mm. Note that the cylinder indented into the finger about 0.4 mm, which was a significant position change with respect to the localization accuracy.

The radius estimate for this experiment seems to have random fluctuations ($< \pm 0.5$ mm) as a function of position. The force estimate has little variation ($< \pm 0.05$ N) and is consistently low, which may be due to a balance beam or model error. Contact location dependencies were not seen.

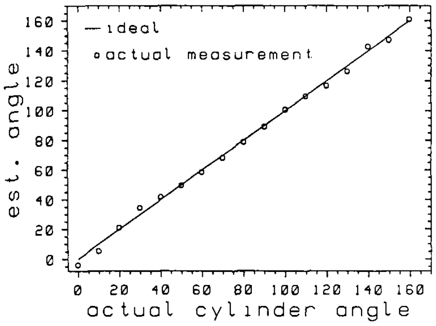

Fig. 14. Sensed orientation for 25-mm-diameter cylinder.

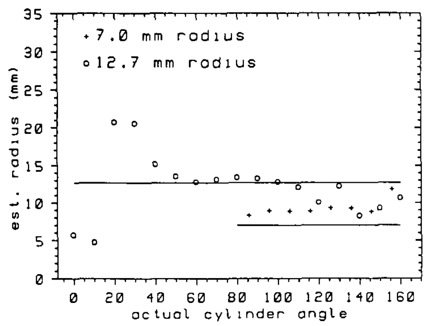

Fig. 15. Radius estimate versus cylinder angle.

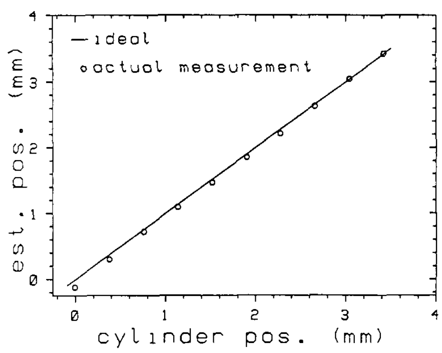

Fig. 16. Tracking cylinder position.

D. Determining Both Principal Curvatures

The previous sections used the cylinder-contact constraint. We now find both curvatures R_B and R'_B (see (6)). Since there is one more parameter to find, we might expect noisier estimates because our measurement set is statistically less adequate. Note that the ellipsoid space (two axes, one orientation, one amplitude) has enough dimensions to be unique for every curvature and force combination. The contact ellipse may be the same for different surfaces, but the amplitude of the ellipsoid will distinguish between them.

Experiments with three spheres are summarized in Table II. The contact ellipse was aligned with the x and y axes, as expected. The curvature error was greater in the circumference direction (R'_B), as expected due to the lower frequency response along y. R'_B for the large sphere was estimated

TABLE II
DETERMINING BOTH PRINCIPAL CURVATURES

Object	R_B	R'_B	Est. R_B	Est. R'_B	rms error
sphere	1.5	1.5	1.1	0.1	2.03%
sphere	18.5	18.5	20.3	22.2	1.77%
sphere	28.5	28.5	25.7	52.8	3.30%
knife	0.2	$\gg 1$	0.5	41.0	3.30%
cyl. edge	≈ 0	12.5	0.6	22.0	4.65%
cylinder	12.5	$\gg 1$	15.5	200.3	1.67%
plane	$\gg 1$	$\gg 1$	150.0	11.7	5.18%
vertex	≈ 0	≈ 0	0.0	0.0	5.08%

rather poorly. The radius error bound for the 28.5-mm-radius sphere in the y direction, $\Delta R'_B$, was found to be eight times the radius error ΔR_B in the x direction. With a 1-N load, the predicted ΔR_B is about 1.5 mm, which explains some of the observed R'_B error. Another error source is the Hertz contact assumptions when contacts are large compared to finger size. The cylinder constraint is not necessary for proper convergence of the least square fit; as seen in Table II for a 25-mm cylinder, we found R within 25% and $R'_B \gg R_B$.

Edges and vertices are interesting features that provide secure grasping points and can be characterized by a very small radius of curvature in at leat one direction (see Table II). For a plane we sensed two large contact radii, but the contact was parallel to the finger axis and therefore suspect. This contact would appear to be the same as a large cylinder aligned with the finger axis. A simple experiment of rotating the finger several degrees ($> \Delta\psi$), and observing that the estimated contact orientation is still aligned with the finger axis, could be used to determine if the contact were with a plane and not a cylinder.

We expect random contacts that are not C^2 to have a larger fitting error since there may not be enough parameters in the Hertz model to adjust. Some preliminary experiments were conducted with a vertex of a cube and the end edge of a cylinder. The algorithm was unable to fit these contacts very well, as shown in Table II. If the contacts are not convex, we should be able to distinguish these cases if the features are further apart than the sensor spacing. Objects that are not C^1 may fit well and be indistinguishable. A good approach might be to evaluate several classes of contact models to see if a better fit could be obtained with one of the classes; however, this has not yet been attempted.

IX. Summary and Future Work

We have shown that a "low-resolution" sensor using only a 4×4 window can give good detail about the surface contact using only a simple elastic analysis with Hertz contact models. Because of the constraint on the expected surface-stress distribution, it is possible to get beyond the linear-filtering spatial-bandwidth limitations to determine the local shape accurately. Using a linear-filter approach, we would need approximately 10 times the sensor density to achieve comparable accuracy.

The curvature determination algorithm was tested on an actual tactile sensor using mainly cylindrical contacts. Experimental results show accurate angle determination to ±3° for cylinders. Radius estimation was fairly good— ± 2 mm or so when the cylinder was at right angles to the finger. Force sensing was the least accurately recovered parameter, although 10% is usable. It would not be easy to servo on the force estimates because of elastic hysteresis and the slowness of the present estimation algorithm.

The experimental conditions tended to give a best case performance. The cylindrical probe was aligned horizontally and normally to be directly above the finger. The forces were large enough to be outside the quantization level but small enough to be close to the sensor's linear range. The probes were smooth, rigid, and polished; thus, the frictionless indentation assumption is reasonable. If there were any tangential surface stresses because the force was applied at an angle, the Hertz contact analysis would need to be modified to include these stresses, as in the analysis by [28].

There are many modeling errors. Gain calibration is only accurate to 5%. Copper strip positioning during fabrication causes sensor position errors. The measured "strains" are really large-scale deflections, not infinitesimal quantities. The separable impulse response model is wrong and can cause problems for contacts that are not along one axis. Surprisingly, we were able to achieve reasonable orientation estimation, despite the simplistic assumptions and models. An *ad hoc* impulse-response model was used; however, it fit well to the experimental data. The most important characteristic of the sensor was that it behaved approximately as a linear system, which made possible the model-based curvature-from-strain inversion. Other empirical models of the sensor (which fit as well) should also perform as well.

The sensor sensitivity and density is adequate for estimating cylinder diameters and orientation, and diameters of small spheres. A weighted average of multiple contacts would improve performance, or the finger orientation could be adjusted to its most sensitive range. However, the goal of this work was to obtain the maximum information from a single contact. The algorithm should be expanded to handle cylinders in alignment with the finger axis and any case where the contact goes to the end of the finger. A new rubber material would reduce hysteresis and increase stability. When the curvature sensing runs in real time, it will be quite useful for high-level tactile feedback with a dextrous robot hand.

Appendix

Contact Shape or Pressure Using Inverse Filtering

In Section III, we fit an empirical impulse response to the discrete strain measurements from the tactile sensor. Can this impulse response be inverted to perform a deconvolution? Here we examine the performance of one-dimensional inverse filters for determining contact shape or surface pressure from strain measurements. There is a linear transform K between surface deflection and measured strain, and a linear transform H between surface stress and measured strain that can be inverted using Fourier transforms:

$$P(s) = H^{-1}(s) E_z(s) \tag{A1a}$$

$$W(s) = K^{-1}(s) E_z(s) \tag{A1b}$$

where s is in cycles per millimeter; $P()$, $W()$, and $E_z()$ are the surface pressure, normal deflection, and strain, respectively, in the frequency domain; and $H^{-1}()$ and $K^{-1}()$ are the inverse frequency responses of the elastic medium for pressure and deflection, respectively. In principle, given adequate sampling density to avoid aliasing, a band-limited surface stress or deflection profile can be recovered from the discrete strain measurements.

The frequency response for the plane-stress model is obtained by taking the Fourier transform of (1) (for depth $d = z$)

$$H(s) = \frac{-1}{E}\left[1 - \upsilon + (1 + \upsilon)2\pi z|s|\right]e^{-2\pi z|s|}. \tag{A2}$$

In the plane-stress model, the deflection at depth z can be obtained by integrating the equation for normal strain $\epsilon_z = \partial w/\partial z$ from ∞ to z. The surface deflection can then be found as a function of the measured strain at depth d [18]

$$\begin{aligned} W(s) &= \frac{2e^{2\pi d|s|}}{2\pi|s|(1 - \upsilon + (1 + \upsilon)2\pi d|s|)} E_z(s) \\ &= K^{-1}(s) E_z(s). \end{aligned} \tag{A3}$$

The surface pressure is obtained from

$$\begin{aligned} P(s) &= \frac{-Ee^{2\pi d|s|}}{(2\pi d|s|(1 + \upsilon) + 1 - \upsilon)} E_z(s) \\ &= H^{-1}(s) E_z(s). \end{aligned} \tag{A4}$$

Both $K^{-1}(s)$ and $H^{-1}(s)$ are ill-behaved functions that grow exponentially with frequency, so they cannot be used directly as inverse filters without band limiting.

The sampling of the strain function puts an upper limit on the frequency response of the inverse filter. For 3.3-mm sampling along the x direction (the sensor spacing along the axis), the antialiasing filter needs a cutoff below 0.15 cycles/mm. By taking repeated measurements as the finger is scanned along a fixed object, the effective sensor density can be increased to reduce the aliasing effects. It is worthwhile to examine the frequency response limitations from the elastic layer above the sensors, in addition to the sampling limits.

We measured the spatial frequency response of the sensor (Fig. 17) by taking the FFT of the impulse response of Fig. 5. If we consider amplitudes $< 1\%$ of the zero frequency signal to be masked by noise, the approximate cutoff frequencies are about 0.25 and 0.15 cycles/mm along the x and y aces, respectively. Any inverse filter must be band limited to this range. The uncertainty principle (see, for example, [5]) implies that the smallest feature obtained from the inverse filter operation would be greater than 4 mm × 6.7 mm. Reducing measurement noise (which is assumed here to be uncorrelated with position, i.e., white) increases the effective cutoff frequency. But the frequency response for a plane-stress model is low pass with a negative exponential in frequency,

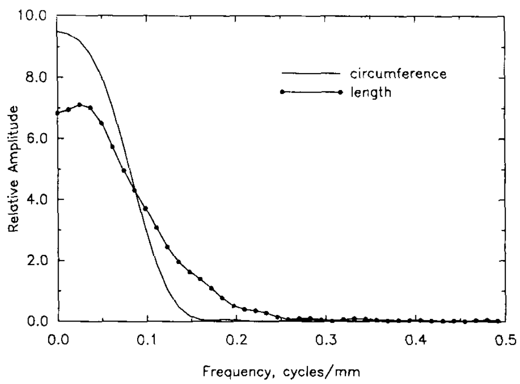

Fig. 17. Measured spatial frequency response of sensor.

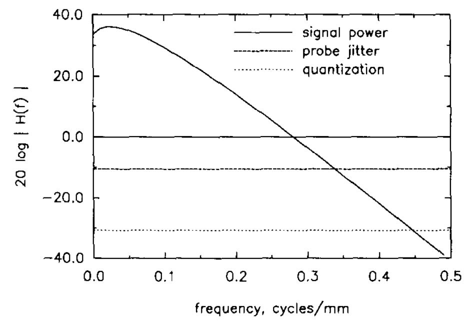

Fig. 18. Power spectrum of sensor response and noise sources.

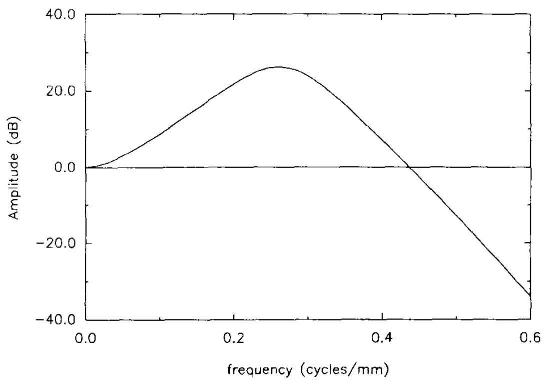

Fig. 19. Inverse (Wiener) pressure restoration filter.

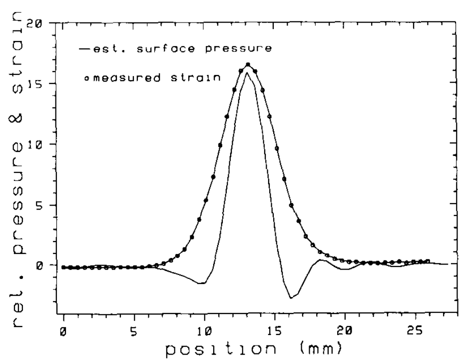

Fig. 20. Inverse filtered knife edge.

so even increasing the signal-to-noise ratio by 40 dB only approximately doubles the cutoff frequency.

Because of undersampling, the inverse filter approach will provide an aliased version of the original input. This aliased version will not necessarily contain the desired curvature information. (See [16] for a discussion of the amplitude and localization errors that result from aliasing.) The pressure signal is reconstructed without any constraint on the form of the pressure distribution. Constraining the desired signal to the limited space of ellipsoidal pressure distributions is shown to be useful in the main body of the paper. The inverse filter approach has merit for the more general shape determination problem, such as the length of a bar pressed into the finger, but the resolution of length is limited by the frequency response of the medium, and aliasing.

Noise Limits to Resolution

In the tactile sensor, the measured strain is in effect a blurred image of the surface pressure. From image processing, a common restoration technique for blurred images is the Wiener filter [25]:

$$\tilde{H}^{-1}(s) = \frac{H^*(s)}{|H(s)|^2 + S_N(s)} \tag{A5}$$

where $\tilde{H}^{-1}(s)$ is the Wiener inverse filter, and $S_N(s)$ is the power spectrum of the noise. We consider a simplistic additive noise model:

$$\hat{\epsilon}_z(x,t) = \epsilon_z(x,t) + e(t) \tag{A6}$$

where $e(t)$ is an additive error. Note (as seen in Fig. 3) that the strain values in the tactile array change significantly over tactel-spacing distances with loads on the order of 0.5 N. These strain values are large with respect to analog–digital converter quantization levels. Thus, we have modeled the error due to quantization with step size $\delta\epsilon_z$ as a uniformly distributed random variable. We make the common assumption that this noise is uncorrelated from sample to sampled [22]. With this assumption, the variance is

$$\sigma_\epsilon^2 = \frac{(\delta\epsilon_z)^2}{12} \tag{A7}$$

and we can assume white noise with a power spectrum

$$S_N(s) = \sigma_\epsilon^2 \approx \frac{(0.1)^2}{12} = 8.3 \times 10^{-4} \tag{A8}$$

where we used the experimentally observed value of $\delta\epsilon_z = \pm 0.05\%$ strain quantization.

One method of increasing the effective sampling density of the sensor is by making subtactel translations of the sensor while taking multiple measurements. However, because the application force has variation for each sample, another noise source is added—the jitter of the force probe. (The force application device is a low-friction balance beam, but measured force can depend on impact velocity and position jitter during initial contact. The standard deviation for the force probe was measured at about 0.3% strain). The noise spectra for probe jitter and quantization error are shown in Fig. 18 superimposed on the power spectrum of the plane-stress response.

The Wiener inverse filter for pressure is shown in Fig. 19 where the noise power $\sigma_\epsilon^2 = 2.5 \times 10^{-3}$ includes probe jitter. The inverse filter de-emphasizes frequencies above which the noise power exceeds the signal power, so the effective cutoff frequency is < 0.5 cycles/mm.

A simple test of the effectiveness of the Wiener inverse filter was conducted. Strain samples from one element were measured as a 0.3-mm knife edge was moved along the finger axis with steps of $\Delta x = 0.51$ mm. The restored pressure distribution in Fig. 20 has a width of about 5.1 mm. The bandwidth limitation due to sensor noise limits the resolution, as expected, to be greater than 4 mm. This resolution is not sufficient for curvature determination because at reasonable contact forces, contacts are not much bigger than this. The model-based method described in the main body can get "super-resolution," well beyond the limits set by linear filtering and the sampling theorem.

Acknowledgment

The authors would like to thank G. Gorali for his excellent work on finger design and construction; B. Armstrong, S. Shekhar, and D. Kriegman for helpful dialogue; and the anonymous reviewers for their helpful comments.

References

[1] P. Akella and M. Cutkosky, "Manipulating with soft fingers: Modelling contacts and dynamics," in *Proc. IEEE Int. Conf. Robotics Automat.* (Scottsdale, AZ), May 1989, pp. 764-769.

[2] P. Allen and R. Bajcsy, "Object recognition using vision and touch," in *Proc. 9th Int. Joint Conf. Artif. Intell.* (Los Angeles), Aug. 1985, pp. 1131-1137.

[3] P. Allen, "Sensing and describing 3-D structure," in *Proc. IEEE Int. Conf. Robotics Automat.* (San Francisco), Apr. 1986, pp. 126-131.

[4] S. Begej, "Planar and finger-shaped optical tactile sensors for robotic applications," *IEEE J. Robotics Automat.*, vol. 4, no. 5, pp. 472-484, Oct. 1988.

[5] R. N. Bracewell, *The Fourier Transform and Its Applications*. New York: McGraw-Hill, 1986.

[6] D. Brock and S. Chiu, "Environment perception of an articulated robot hand using contact sensors," in *Proc. ASME Winter Ann. Meeting* (Miami, FL), 1985, pp. 89-96.

[7] A. Cameron, R. Daniel, and H. Durrant-Whyte, "Touch and motion," in *Proc. IEEE Int. Conf. Robotics Automat.* (Philadelphia, PA), Apr. 1988, pp. 1062-1067.

[8] D. H. Cooper, "Hertzian contact-stress deformation coefficients," *J. Appl. Mech.*, vol. 36, no. 2, pp. 296-303, June 1969.

[9] M. R. Cutkosky, "Mechanical properties for the grasp of a robotic hand," CMU Robotics Institute Tech. Rep. CMU-RI-TR-84-24, 1984.

[10] P. Dario, M. Bergamasco, D. Femi, A. Fiorillo, and A. Vaccarelli, "Tactile perception in unstructured environment: A case study for rehabilitative robotics applications," in *Proc. IEEE Int. Conf. Robotics Automat.* (Raleigh, NC), Apr. 1987, pp. 2047-2054.

[11] M. R. Driels, "Pose estimation using tactile sensor data for assembly operations," in *Proc. IEEE Int. Conf. Robotics Automat.* (San Francisco), Apr. 1986, pp. 1255-1261.

[12] R. S. Fearing and J. M. Hollerbach, "Basic solid mechanics for tactile sensing," *Int. J. Robotics Res.*, vol. 4, no. 3, Fall 1985.

[13] R. S. Fearing, A. Rise, and T. O. Binford, "A tactile sensing finger tip for a dextrous hand," in *Proc. SPIE Conf. Intell. Robotics Comput. Vision* (Cambridge, MA), Oct. 1986, pp. 378-387.

[14] R. S. Fearing, "Some experiments with tactile sensing during grasping," in *Proc. IEEE Int. Conf. Robotics Automat.* (Raleigh, NC), Apr. 1987, pp. 1637-1643.

[15] —, "Tactile sensing, perception, and shape interpretation," Ph.D. dissertation, Dept. of Elec. Eng., Stanford Univ., Stanford, CA, Dec. 1987.

[16] —, "Tactile sensing mechanisms," *Int. J. Robotics Res.*, vol. 9, no. 3, pp. 3-23, June 1990.

[17] K. L. Johnson, *Contact Mechanics*. New York: Cambridge, 1985.

[18] G. M. L. Gladwell, *Contact Problems in the Classical Theory of Elasticity*. Amsterdam, The Netherlands: Sitjhoff and Nordhoff, 1980.

[19] S. J. Gordon and W. P. Seering, "Accuracy issues in measuring quantized images of straight-line features," in *Proc. IEEE Int. Conf. Robotics Automat.* (San Francisco), Apr. 1986, pp. 931-936.

[20] V. S. Gurfinkel, A. Yu. Shneyder, Ye. M. Kanayev, and Ye. V. Gurfinkel, "Tactile sensitizing of manipulators," *Eng. Cybern.*, vol. 12, no. 6, pp. 47-56, Nov. 1974.

[21] D. J. Montana, "Tactile sensing and the kinematics of contact," Ph.D. dissertation, Div. of Appl. Sci., Harvard Univ., Cambridge, MA, 1986.

[22] A. V. Oppenheim and R. W. Schafer, *Digital Signal Processing*. Englewood Cliffs, NJ: Prentice-Hall, 1975.

[23] Y. C. Pati, D. Friedman, P. S. Krishnaprasad, C. T. Yao, M. C. Peckerar, R. Yang, and C. R. K. Marrian, "Neural networks for tactile perception," in *Proc. IEEE Int. Conf. Robotics Automat.* (Philadelphia, PA), Apr. 1988, pp. 134-139.

[24] J. Ponce, D. Chelberg, and W. Mann, "Invariant properties of straight homogeneous generalized cylinders and their contours," *IEEE Trans. Pattern Anal. Machine Intell.*, vol. 11, no. 9, pp. 951-966, Sept. 1989.

[25] W. K. Pratt, *Digital Image Processing*. New York: Wiley, 1978.

[26] S. Shekhar, O. Khatib, and M. Shimojo, "Sensor fusion and object localization," in *Proc. IEEE Int. Conf. Robotics Automat.* (San Francisco), Apr. 1986, pp. 1623-1628.

[27] D. M. Siegel, "Contact sensors for dextrous robotic hands," MIT AI Lab Tech. Rep. 900, June 1986.

[28] J. O. Smith and C. K. Liu, "Stresses due to the tangential and normal loads on an elastic solid with application to some contact stress problems," *J. Appl. Mech., Trans. ASME*, vol. 75, pp. 157-166, June 1953.

[29] T. H. Speeter, "Analysis and control of robotic manipulation," Ph.D. dissertation, Dept. of Biomed. Eng., Case Western Reserve Univ., Jan. 1987.

[30] G. Strang, *Linear Algebra and its Applications*. San Diego, CA: Harcourt Brace Jovanovich, 1980.

[31] G. B. Thomas, *Calculus and Analytic Geometry*. Reading, MA: Addison-Wesley, 1968.

[32] S. Timoshenko and J. N. Goodier, *Theory of Elasticity*. New York: McGraw-Hill, 1951.

[33] R. Yang, "Tactile perception for multifingered hands," SRC TR 87-162, Univer. Maryland, Systems Res. Center, 1987.

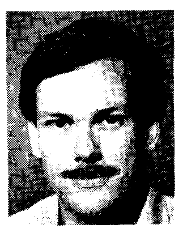

Ronald S. Fearing (S'84–M'87) received the S.B. and S.M. degrees from the Massachusetts Institute of Technology, Cambridge, in 1983 and the Ph.D. degree in electrical engineering from Stanford University, Stanford, CA. His dissertation concerned robotic tactile sensing.

He has been at the Electrical Engineering and Computer Sciences Department at the University of California, Berkeley, since January 1988, where he is currently an Assistant Professor. His research interests are in tactile sensing, dextrous manipulation, microrobots, and natural intelligence.

Dr. Fearing received the Presidential Young Investigator Award in 1991.

T. O. Binford, photograph and biography not available at the time of publication.